Proceedings of the ASME 2013 Pressure Vessels and Piping Conference
PVP2013
July 14-18, 2013, Paris, France

PVP2013-97211

EVALUATION OF DUCTILE TEARING OF X-80 PIPELINE GIRTH WELDS USING SE(T), SE(B) AND C(T) FRACTURE SPECIMENS

Leonardo L. S. Mathias
Dept. of Naval Arch. and Ocean Eng.
University of São Paulo
São Paulo, SP 05508-900, Brazil
Email: leonardomathias@usp.br

Diego F. B. Sarzosa
Dept. of Naval Arch. and Ocean Eng.
University of São Paulo
São Paulo, SP 05508-900, Brazil
Email: dsarsoza@usp.br

Claudio Ruggieri
Dept. of Naval Arch. and Ocean Eng.
University of São Paulo
São Paulo, SP 05508-900, Brazil
Email: claudio.ruggieri@poli.usp.br

ABSTRACT

Structural integrity assessments of pipe girth welds play a key role in design and safe operation of piping systems, including deep water steel catenary risers. Current methodologies for structural integrity assessments advocate the use of geometry dependent resistance curves so that crack-tip constraint in the test specimen closely matches the crack-tip constraint for the structural component. Testing standards now under development to measure fracture resistance of pipeline steels (*J* and CTOD) most often employ single edge notched specimens under tension (SENT) to match a postulated defect in the structural component. This paper presents an investigation of the ductile tearing properties for a girth weld of an API 5L X80 pipeline steel using experimentally measured crack growth resistance curves (*J*-*R* curves). Testing of the girth weld pipeline steels employed clamped SE(T) specimen with center-crack weld and three-point bending SE(B) (or SENB) specimens to determine the *J*-*R* curves. Tests involving SE(B) specimens are usually considered conservative, however, the comparison between this two methods may point an accurate alternative for girth weld assessments, since adequate geometry is adopted to describe accurately the structure's behavior.

INTRODUCTION

Predictive methodologies aimed at quantifying the impact of defects in oil and gas pipelines play a key role in safety assessment procedures (such as, for example, repair decisions and life-extension programs) of in-service facilities. The pipe reeling process is currently the most efficient and fast installation method employed by the offshore industry [1,2]. Pipes are welded still at onshore facility, and coiled around a large diameter reel on a vessel, and then unreeled, straightened and deployed to the sea floor. Use of high strength steel pipelines is motivated by the increasing demand in the number of applications for the oil and gas industry, including marine applications and steel catenary risers. This process involves high bending stresses and therefore subjects the pipeline system to plastic deformation (around 2~3%), which affects directly the flaw acceptance criteria for the pipe and girth welds.

Fracture mechanics based approaches to describe ductile fracture behavior in structural components, including welded structures, rely upon crack growth resistance (*J*-Δa) curves (also termed *R*-curves) to characterize crack extension followed by crack instability of the material [3,4]. Current standards [5] employ specimens which provide too conservative results that, consequently, put severe limitations on the application for high strength materials. Such conservativeness would hardly allow

flaws in the structure, leading to unnecessary repairs that could take time and be very expensive.

Recent applications of SE(T) fracture specimens to characterize crack growth resistance properties in pipeline steels [6-14] have been effective in providing larger flaw tolerances while, at the same time, reducing the otherwise excessive conservatism which arises when measuring the material's fracture toughness based on high constraint, deeply-cracked, single edge notch bend (SE(B)) or compact tension (C(T)) specimens. However, some difficulties associated with SE(T) testing procedures raise concerns about the significance and qualification of measured crack growth resistance curves. Testing of shallow-crack bend specimens (which is a nonstandard SE(B) configuration) may become more attractive due to its simpler testing protocol, laboratory procedures and much smaller loads required to propagate the crack. Consequently, use of smaller specimens which yet guarantee adequate levels of crack-tip constraint to measure the material's fracture toughness becomes an attractive alternative.

This work presents an investigation of the ductile tearing properties, in terms of geometry dependence (shallow *vs*. deep cracked), loading mode (tension *vs*. bending) and weld strength mismatch, of an API 5L X80 pipeline girth weld using experimentally measured crack growth resistance curves (*J-Δa* curves). Testing of the pipeline girth welds employed side-grooved, clamped SE(T), 3-Point bend SE(B) and C(T) specimens with a weld centerline notch to determine the crack growth resistance curves based upon the unloading compliance (UC) method using a single specimen technique. This experimental characterization provides additional toughness data which serve to evaluate crack growth resistance properties of pipeline girth welds using SE(T) and SE(B) specimens with weld centerline cracks.

EXPERIMENTAL PROGRAM

Material Description

The base material utilized in this study was a high strength, low allow (HSLA) API grade X80 pipeline steel with 20-inch diameter and wall thickness, t_w = 19 mm .Pipe was produced as a base plate using a control-rolled processing route without accelerated cooling. Table 1 provides the mechanical properties of the base plate and weld metals, measured by sub sized specimens based on standard tensile testing according to ASTM A370 [15]. Yield strength data from Table 1 reveal an approximately 18% overmatched weld condition.

Girth welding was performed using the FCAW process in the 1G (flat) position with a single V-groove configuration in which the root pass was made by GMAW welding. Using Annex F of API 579 [16], the Ramberg-Osgood strain hardening exponents describing the stress-strain response for the baseplate and weld metal are estimated as n_{BM} = 20.3 and n_{WM}=35.2.

Table 1 *Material properties of the base plate and weldment for the tested pipeline girth weld.*

Base Plate			Weld		
σ_{ys} (MPa)	σ_{uts} (MPa)	n	σ_{ys} (MPa)	σ_{uts} (MPa)	n
609	679	20.3	716	750	35.2

Specimen Geometry

Figure 1 illustrates SE(T) and SE(B) specimens geometry. Both geometries are squared cross-sectioned, with B=W=14.8 mm. Clamped SE(T) specimens have a/W = 0.4 and clamp distances H = 88.8 and 148 mm, which provides H/W = 6 and 10, respectively (refer to Fig. 1(a)). Here, a denotes the crack depth and W the specimen width, which is slightly smaller than the pipe thickness, t_w. Tests involving SE(B) specimens with a/W = 0.25 and spam S = 4W (refer to Fig. 1(b)), and C(T) specimens with B = 14 mm and W = 4B (both are nonstandard configurations) were also conducted. SE(B) and SE(T) specimens were precracked using a 3-point bend apparatus very similar to a conventional 3-point bend test. C(T) specimens were precracked according to recommendations of ASTM E1820 [5]. After fatigue pre-cracking, all specimens were side-grooved to a net thickness of ~ 85% of the overall thickness (7.5% side-groove on each side) to promote uniform crack growth. Tests were conducted following some general guidelines described in ASTM E1820 standard [5]. Records of load *vs*. crack mouth opening displacements (CMOD) were obtained from the specimens using a clip gauge mounted on knife edges attached to the specimen surface.

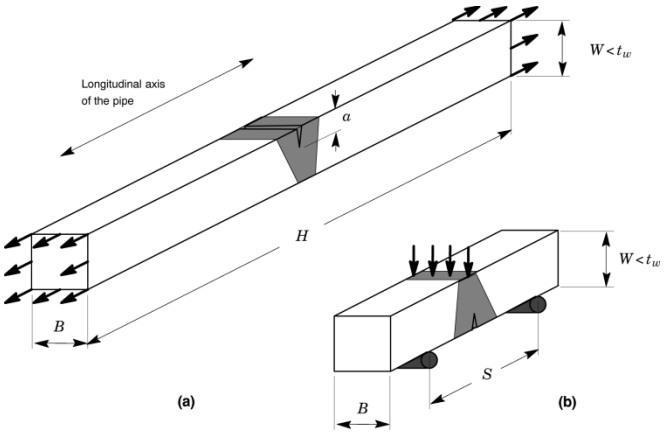

Figure 1 – *Geometry of tested fracture specimens with weld centerline notch. (a) Clamped SE(T) specimen with a/W = 0.4 and H/W = 6 and 10; (b) 3-Point SE(B) specimen with a/W = 0.25 and S/W = 4. (BxB) configuration was employed.*

ESTIMATION PROCEDURE OF *J-R* CURVES

J-integral can be conveniently defined in terms of its elastic component, J_e, and plastic component, J_p, as

$$J = J_e + J_p = \frac{K_I^2}{E'} + \frac{\eta A_p}{B_N b} \quad (1)$$

where K_I is the elastic stress intensity factor for the cracked configuration, A_p is the plastic area under the load-displacement curve, B_N is the net specimen thickness at the side groove roots ($B_N = B$ if the specimen has no side grooves where B is the specimen gross thickness), b is the uncracked ligament ($b = W - a$ where W is the width of the cracked configuration and a is the crack length). In writing the first term of Eq. (1), plane-strain conditions are adopted such that $E' = E/(1 - \upsilon^2)$ where E and υ are the (longitudinal) elastic modulus and Poisson's ratio, respectively.

Factor η represents a nondimensional parameter which relates the plastic contribution to the strain energy for the cracked body and *J*. Figure 2 illustrates the essential features of the estimation procedure for J_p. A_p (and consequently η) is defined in terms of load-load line displacement (LLD or Δ) data or load-crack mouth opening displacement (CMOD or V) data. Measuring methods of LLD and CMOD are schematically illustrated in Fig. 2(b) (see details about the difference between CMOD and LLD in [8]). For definiteness, these quantities are denoted η^{CMOD} and η^{LLD}.

The previous Eq. (1) defines the key quantities driving the evaluation procedure for *J* as a function of applied (remote) loading and crack size. However, the area under the actual load-displacement curve for a growing crack differs significantly from the corresponding area for a stationary crack (which the deformation definition of *J* is based on) [2]. Consequently, the measured load-displacement records must be corrected for crack extension to obtain an accurate estimate of *J*-values with increased crack growth (see further details in [8]). A widely used approach (which forms the basis of current standards such as ASTM E1820 [5]) to evaluate *J* with crack extension follows from an incremental procedure which updates J_e and J_p at each partial unloading point, denoted k, during the measurement of the load *vs.* displacement curve illustrated in Fig. 2 in the form

$$J_k = J_e^k + J_p^k \quad (3)$$

where the current elastic term is simply given by

$$J_e^k = \frac{\left(K_I^k\right)^2}{E'} \quad (4)$$

For the SE(B) and C(T) configurations analyzed here, solutions for K_I can be found in several previously published works, such as Tada et al. [17], whereas Cravero and Ruggieri [7] provide K_I solutions for clamped SE(T) specimens.

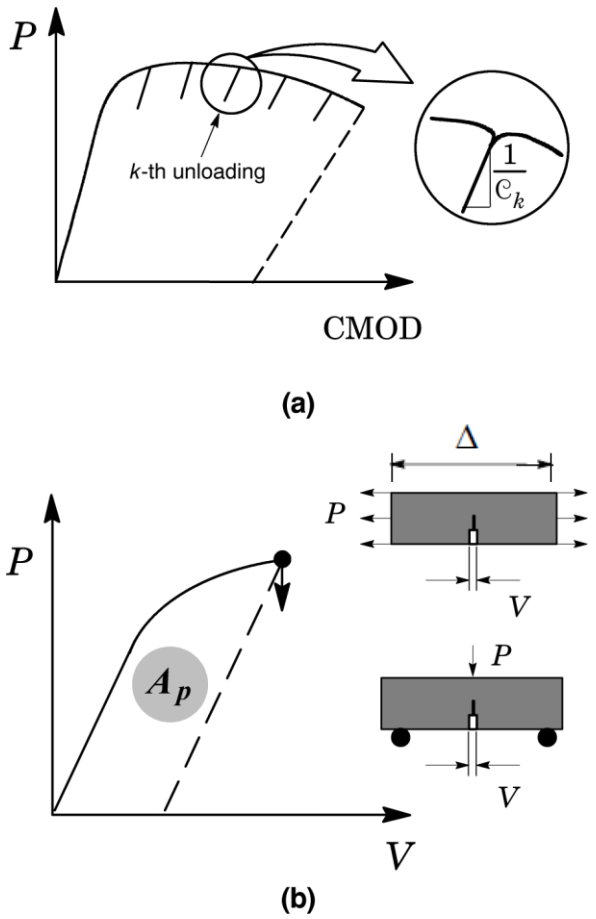

Figure 2 *(a) Partial unloading during the evolution of load with crack mouth opening displacement; (b) Definition of the plastic area under the load-displacement curve, determined in terms of LLD (Δ) or CMOD (V).*

Evaluation of the plastic term, J_p^k, deserves further discussion. Early methods to measure *J*-resistance curves adopted an incremental equation to estimate J_p based entirely on load-load line displacement (LLD) records which derives from the fundamental work of Ernst et al. [18]. In addition to the η-factor introduced previously, the approach relies on a geometric factor to correct the incremental plastic work for crack growth. Given the conditions of *J*-controlled crack growth and deformation plasticity are satisfied, the methodology enables accurate estimations of J_p for arbitrary (small) increments of crack length and load line displacement. However, when crack growth response is measured using load-crack mouth opening displacement (CMOD) records, direct application of Ernst's incremental formulation to evaluate J_p at each partial unloading point does not hold true. Recognizing this limitation, Cravero and Ruggieri [8] and Zhu et al. [19] introduced an incremental formulation to determine J_p which is more applicable to CMOD data in the form

$$J_p^k = \left[J_p^{k-1} + \frac{\eta_{k-1}^{CMOD}}{b_{k-1} B_N} \left(A_p^k - A_p^{k-1} \right) \right] \times \Gamma \quad (5)$$

in which Γ is defined as

$$\Gamma = 1 - \frac{\gamma_{k-1}^{LLD}}{b_{k-1}} \left(a_k - a_{k-1} \right) \quad (6)$$

where factor γ^{LLD} is evaluated from

$$\gamma_{k-1}^{LLD} = \left[-1 + \eta_{k-1}^{LLD} - \left(\frac{b_{k-1}}{W \eta_{k-1}^{LLD}} \frac{d\eta_{k-1}^{LLD}}{d(a/W)} \right) \right] \quad (7)$$

The incremental expression for J_p, defined by Eqs. (5-7), contains two contributions: one is from the plastic work in terms of CMOD and, hence, η^{CMOD} and the other is due to crack growth correction in terms of LLD by means of η^{LLD}. While the resulting *J*-estimation procedure based on CMOD may appear a little more complex, evaluation of Eq. (5) coupled with Eqs. (6, 7) is also relatively straightforward provided the two geometric factors, η^{CMOD} and η^{LLD}, are known (see details about the difference and the relation of LLD and CMOD in [8]). Further section addresses crack growth resistance testing of fracture specimens with different geometries which include: 1) clamped SE(T) specimen; 2) nonstandard SE(B) specimen and 3) C(T) specimen. The corresponding η-factor equations are provided in the following subsections.

Clamped SE(T) Specimens

Single edge-notched tension specimens (SE(T)) with fixed-grip loading have been increasingly used in crack growth resistance measurements for key structural applications, including girth weld defect assessments in oil and gas transmission pipelines and submarine risers. Because this specimen is a nonstandard ASTM configuration, only a few previous studies [6,7,9,20,21,22] have developed wide range *J* estimation equations for SE(T) geometries based on η-factors. In related work, Cravero and Ruggieri [7] and Ruggieri [22] provide an extensive body of results covering η^{CMOD} and η^{LLD} values for different hardening properties and varying *a/W* and *H/W* ranges. To facilitate manipulation of their results while, at the same time, providing a more direct evaluation procedure, the functional dependence of the η-factor with crack size and clamp distance can be rewritten in simpler forms summarized as follows

$$\eta_{SET(\frac{H}{W})=6}^{CMOD} = 1.081 - 2.219\left(\frac{a}{W}\right) + 11.897\left(\frac{a}{W}\right)^2 - 35.689\left(\frac{a}{W}\right)^3 + 46.633\left(\frac{a}{W}\right)^4 - 21.792\left(\frac{a}{W}\right)^5 \quad (8)$$

$$\eta_{SET(\frac{H}{W})=6}^{LLD} = -1.027 + 19.906\left(\frac{a}{W}\right) - 72.889\left(\frac{a}{W}\right)^2 + 126.378\left(\frac{a}{W}\right)^3 - 107.534\left(\frac{a}{W}\right)^4 + 35.801\left(\frac{a}{W}\right)^5 \quad (9)$$

$$\eta_{SET(\frac{H}{W})=10}^{CMOD} = 1.067 - 1.767\left(\frac{a}{W}\right) + 7.808\left(\frac{a}{W}\right)^2 - 18.269\left(\frac{a}{W}\right)^3 + 15.295\left(\frac{a}{W}\right)^4 - 3.083\left(\frac{a}{W}\right)^5 \quad (10)$$

$$\eta_{SET(\frac{H}{W})=10}^{LLD} = -0.623 + 9.336\left(\frac{a}{W}\right) - 4.584\left(\frac{a}{W}\right)^2 - 47.963\left(\frac{a}{W}\right)^3 + 87.697\left(\frac{a}{W}\right)^4 - 44.875\left(\frac{a}{W}\right)^5 \quad (11)$$

where it is understood that a 5-th order polynomial fitting valid in the range $0.2 \le a/W \le 0.7$ is followed.

3-Point SE(B) Specimens

Research efforts to improve fracture toughness testing methods based on conventional SE(B) specimens (with *Bx2B* configuration) have recently introduced revised *J*-integral equations and improved η-factors [23-27]. Here, we use an appropriate polynomial fitting to describe the results provided by Donato and Ruggieri [25] which allows defining the η-factors for SE(B) specimens as

$$\eta_{SEB}^{CMOD} = 3.650 - 2.111\left(\frac{a}{W}\right) + 0.341\left(\frac{a}{W}\right)^2 \quad (12)$$

$$\eta_{SEB}^{LLD} = 0.020 + 18.086\left(\frac{a}{W}\right) - 73.246\left(\frac{a}{W}\right)^2 + 152.225\left(\frac{a}{W}\right)^3 - 159.769\left(\frac{a}{W}\right)^4 + 66.879\left(\frac{a}{W}\right)^5 \quad (13)$$

which are valid in the range $0.1 \le a/W \le 0.7$. The above equations agree very well with the revised *J*-integral expressions developed by Zhu and Joyce [26] which form the basis of current ASTM E1820 standard using CMOD records [5].

C(T) Specimens

Early work to develop a single-specimen experimental procedure for laboratory measurements of *J* [28] focused on the utilization of compact tension C(T) specimens. However, ASTM E1820 [5] specifies a cut-out added to the standard C(T) geometry of the early ASTM E399 [29] thereby allowing measurement of the load line displacement as the crack mouth opening displacement. Consequently, the *J*-integral formulations, including the compliance equations to estimate crack length discussed next, are valid only for LLD measurements. When the standard C(T) configuration is utilized and CMOD records are measured in the test procedure, additional equations defining the functional dependence of factor η with crack size are needed.

Recent work of Savioli and Ruggieri [30] arrive at the following set of equations for the η-factors. Difference in Eqs. (14) and (15) are basically due to the location in the specimen taken for measurement records (further details in [30])

$$\eta_{CT}^{CMOD} = -2.264 + 18.244\left(\frac{a}{W}\right) - 26.430\left(\frac{a}{W}\right)^2 + 12.124\left(\frac{a}{W}\right)^3 \quad (14)$$

$$\eta_{CT}^{LLD} = -1.699 + 19.807\left(\frac{a}{W}\right) - 30.118\left(\frac{a}{W}\right)^2 + 14.099\left(\frac{a}{W}\right)^3 \quad (15)$$

which are valid in the range $0.45 \leq a/W \leq 0.7$.

Estimation of Crack Extension

Current testing protocols to measure the crack growth resistance response using a single-specimen test are primarily based on the unloading compliance (UC) technique to estimate the (current) crack length from the specimen compliance measured at periodic unloadings with increased deformation. Figure 2(a) illustrates the essential features of the method. The slope of the load-displacement curve during the *k-th* unloading defines the current specimen compliance, denoted C_k ($C=V/P$, where V is the CMOD and P represents the applied load), which depends on specimen geometry and crack length. For the crack configurations analyzed here. the specimen compliance based on CMOD is most often defined in terms of normalized quantities expressed as

$$\mu_{CMOD}^{SE(T)}, \mu_{CMOD}^{C(T)} = \frac{1}{1+\sqrt{EB_eC}} \quad (16)$$

and

$$\mu_{CMOD}^{SE(B)} = \left[\frac{\sqrt{WEB_eC}}{S/4} + 1\right]^{-1} \quad (17)$$

where μ_{CMOD}^{SET}, μ_{CMOD}^{CT} and μ_{CMOD}^{SEB} define the normalized compliances for the SE(T), C(T) and SE(B) specimens. In the above expressions, E is the longitudinal elastic modulus, and B_e the effective thickness is defined by

$$B_e = B - \frac{(B-B_N)^2}{B} \quad (18)$$

According to Eq.16, the same μ-expression is used for C(T) and SE(T) specimens. However, their μ values will differ significantly, because of the dependence of C_k. By measuring the instantaneous compliance during unloading of the specimen illustrated in Fig. 2(b), the current crack length follows directly from solving the functional dependence of crack length and specimen compliance in terms of μ_{CMOD}. Cravero and Ruggieri [7] and current ASTM 1820 [5] provides results for μ_{CMOD}^{SET} and μ_{CMOD}^{SEB} written in the form

$$a/W = \sum_{i=0}^{5} \beta_i \mu^i \quad (19)$$

which β-coefficients are displayed on Table 1.

Table 1 *Coefficients of crack extension estimation expressions in terms of normalized compliance for SE(T) and SE(B) specimens*

Coefficient	SE(T) $_{H/W=10}$	SE(T) $_{H/W=6}$	SE(B)
β_0	1.9215	2.1509	0.9997
β_1	-13.2195	-13.2405	-3.9504
β_2	58.7080	48.8649	2.9821
β_3	-155.2823	-110.8908	-3.2141
β_4	207.3987	131.1808	51.5164
β_5	-107.9176	-61.2957	-113.0310

We now direct attention to the unloading compliance testing of the C(T) specimen. As already noted, the compliance equations to estimate crack length given by ASTM 1820 [5] are applicable to LLD measurements only. Use of the standard C(T) configuration requires an additional compliance equation to estimate the crack length from CMOD measurements which is provided by Ruggieri [31] as

$$\left(\frac{a}{W}\right)_{CT} = 0.9368 - 2.1607\mu - 19.3666\mu^2 + 57.5279\mu^3 \quad (20)$$

with $0.40 \leq a/W \leq 0.7$.

Effects of Weld Strength Overmatch on η-Factors

Current test standards employ J estimation expressions which are mainly applicable to fracture specimens made of homogeneous materials. For a given specimen geometry, mismatch between the weld metal and base plate strength affects the macroscopic mechanical behavior of the specimen in terms of its load-displacement response with a potentially strong impact on the coupling relationship between J and the near-tip stress fields. Accurate estimation formulas for J more applicable to welded fracture specimens may become important in robust defect assessment procedure capable of including effects of weld strength mismatch on fracture toughness.

Previous work of Donato et al. [32], Paredes and Ruggieri [22] and Savioli and Ruggieri [30] introduce a functional dependence of factor η^{CMOD} with crack size and strength mismatch level for the tested fracture specimens which are summarized as follows

$$\eta_{SET}^{CMOD} = -0.356 + 11.686\left(\frac{a}{W}\right) - 23.589\left(\frac{a}{W}\right)^2 + 13.899\left(\frac{a}{W}\right)^3 - 0.276M_y - 0.034{M_y}^2 \quad (21)$$

$$\eta_{SEB}^{CMOD} = 3.882 + 0.222\left(\frac{a}{W}\right) - 5.012\left(\frac{a}{W}\right)^2 + 4.021\left(\frac{a}{W}\right)^3 - 0.407M_y - 0.050{M_y}^2 \quad (22)$$

$$\eta_{CT}^{CMOD} = -3.864 + 29.086\left(\frac{a}{W}\right) - 46.404\left(\frac{a}{W}\right)^2 + 24.415\left(\frac{a}{W}\right)^3 - 0.252M_y - 0.106{M_y}^2 \quad (23)$$

where the mismatch ratio, M_y, ranges between 1.0 (evenmatch) and 1.5 (50% overmatch) and is defined by

$$M_y = \frac{\sigma_{YS}^{MS}}{\sigma_{YS}^{MB}} \quad (24)$$

RESULTS AND DISCUSSION

Crack Growth Resistance Curves

This section presents the crack growth resistance curves evaluated from the X80 pipeline girth weld based on laboratory measurements of load and CMOD for the employed geometries. Figure 3 shows a typical load-displacement curve measured from testing the SE(T) specimen and the shallow crack SE(B) configuration. The strong effect of loading mode (tension *vs*. bending) associated with specimen geometry is evident in this plot. At similar levels of CMOD, the applied load for the SE(T) specimen increases approximately by a factor of 4 compared to the load response for the SE(B) specimen.

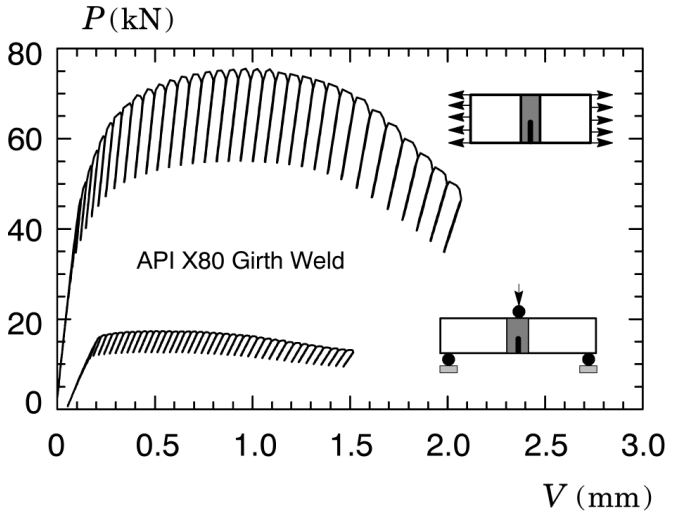

Figure 3 *Measured load-CMOD curve for the tested X80 pipeline girth weld using clamped SE(T) specimens with a/W=0.4 and 3-Point SE(B) specimens with a/W=0.25*

Figures 4-8 show the measured resistance curves for the tested crack configurations with different specimen geometries and *a/W*-ratios. Consider first the effect of crack growth correction on the resistance curves for the SE(T) specimen with *H/W*=10 displayed in Figs. 4 and 5. These two sets of curves show that crack growth correction lowers the measured fracture resistance for a given *Δa*-value, particularly for increased crack extension. Here, the fracture resistance measured in terms of *J* for the results with crack growth correction shown in Fig. 5 is reduced by 10~15% for $\Delta a \geq 2$ mm compared to the results displayed in Fig. 4. Very similar trends are observed for the measured resistance curves obtained from other fracture specimens. Since the focus here lies on comparisons of *J-Δa* response for different crack configurations, the results described subsequently are derived from using the crack growth correction term to determine *J*.

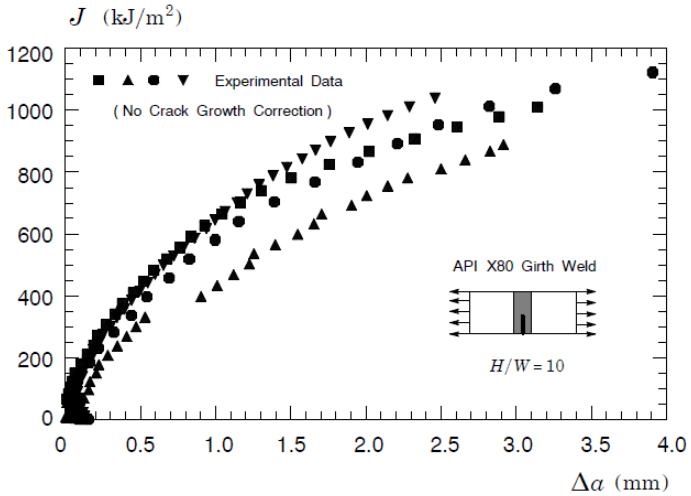

Figure 4 *Measured J-R curves for the tested X80 pipeline girth weld using clamped SE(T) specimens with a/W=0.4, H/W=10 with no crack growth correction*

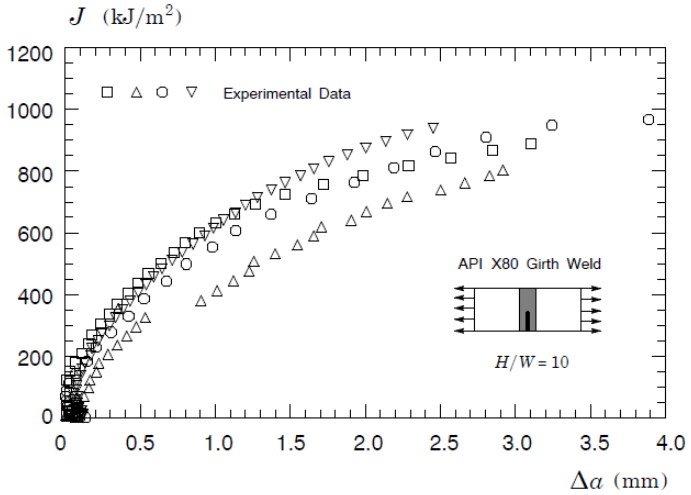

Figure 5 *Measured J-R curves for the tested X80 pipeline girth weld using clamped SE(T) specimens with a/W=0.4, H/W=10 with crack growth correction*

Figure 6 displays the *J*-resistance curves for the SE(T) specimen with *H/W*=6. It is seen that the measured crack growth response for this configuration is essentially similar to the previous resistance curves for the SE(T) specimen with *H/W*=10 shown in Fig. 5. It is evident the little influence, if any, of the clamp distance, *H*, on the *J-R* curves for this specimen configuration within the tested *H/W* range. A small effect of the *H/W*-ratio on the average slope of the resistance curves is also noticed with slightly higher slopes observed in the experimental data for the configuration with *H/W*=6. However, such differences can be considered minimal since all

resistance curves lie within the inherent material variability of the measured data band.

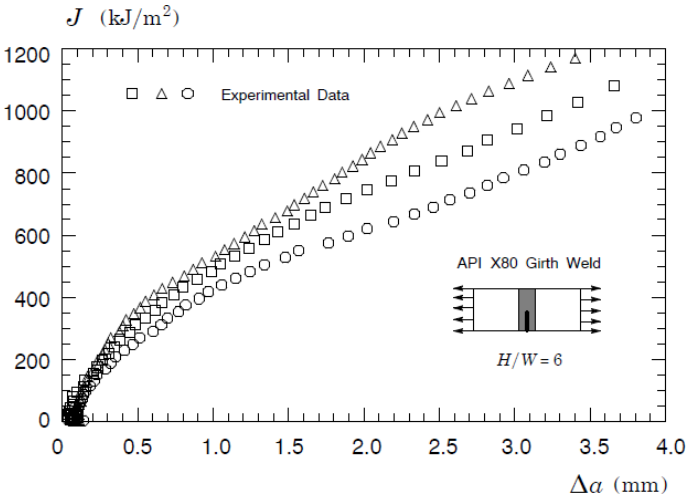

Figure 6 *Measured J-R curves for the tested X80 pipeline girth weld using clamped SE(T) specimens with a/W=0.4, H/W=6*

Figure 7 shows the crack growth response for the shallow crack SE(B) specimens. Unfortunately, the measured resistance curves are perhaps somewhat more scattered that we would expect for these specimens. Moreover, some of the tested bend specimens exhibited reduced ductile crack growth at test termination to about 1 mm compared to the other specimens without, however, no appreciable reduction in *J*-values. While we did not investigate thoroughly such behavior, the crack front measurements addressed later in further section reveal a rather highly uneven crack advance, thus providing some explanation for the shape of the measured resistance curves. However, it is nevertheless evident that the *J*-resistance data for the SE(B) configuration compare well with the SE(T) specimen results.

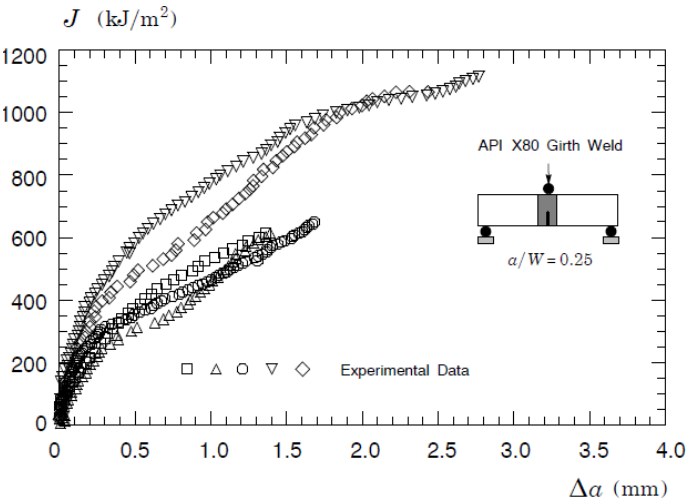

Figure 7 *Measured J-R curves for the tested X80 pipeline girth weld using SE(B) specimens with a/W=0.25*

Figure 8 provides a summary plot which emphasizes the effect of specimen geometry on the crack growth resistance behavior for the tested API X80 girth weld. The plot also includes the measured resistance curves for the C(T) specimen with *a/W*=0.5; this crack configuration has the highest crack-tip constraint thereby producing the lowest *J-Δa* response. To facilitate comparison, only the lowest and highest resistance curves for the shallow crack SE(B) specimen and SE(T) configuration with *H/W*=10 are included in the plot; these curves can therefore be interpreted as the measured data band for these specimens.

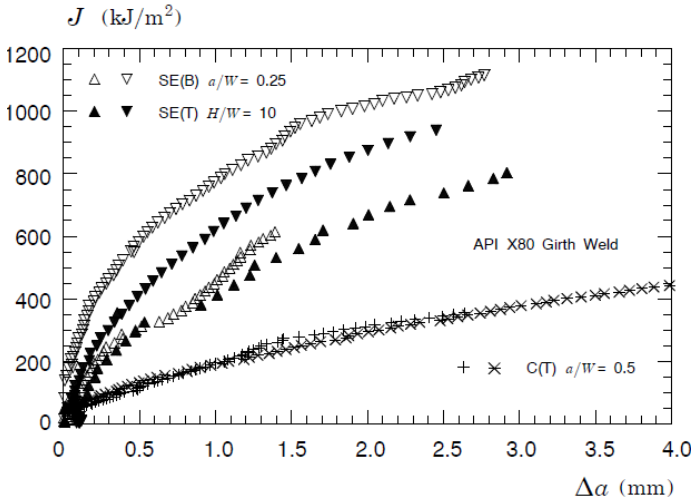

Figure 8 *Effects of geometry dependence on J-R curves for the tested X80 pipeline girth weld using clamped SE(T), shallow crack SE(B), and C(T) specimens*

As already observed, an evident feature emerging from these results is that there appears to be little geometry dependence of the *J*-resistance curves for the shallow crack SE(B) and SE(T) specimens. Indeed, the approximate average *J-R* curve for the shallow crack SE(B) specimen is actually slightly higher that the corresponding average *J-Δa* response for the SE(T) configuration. This result, however, should not be uncritically endorsed since, as discussed previously, the crack growth resistance data for the SE(B) specimen exhibited larger scatter associated with uneven crack advance which may diminish a little the rigor of the comparison. Further, there is a striking difference between the *J*-resistance curves for the deeply-cracked C(T) specimens and the SE(B) and SE(T) configurations, a behavior that was already anticipated. It can be reasonably concluded from the results displayed in this plot that, while the C(T) specimen provides very low *J*-resistance curves, crack growth response is likely to be sufficiently describable by either the shallow crack SE(B) specimen and the SE(T) specimen to serve as a basis for ductile tearing assessments in ECA procedures applicable to pipeline girth welds and similar structural components.

Effects of Weld Strength Overmatch on J-R Curves

This section examines the effect of weld strength mismatch on the fracture resistance as measured by the *J-Δa* response for the tested SE(T) and SE(B) specimens with weld centerline notch. The primary objective is to gain further insight into the potential deviation that arises from evaluating the *J*-resistance curves using η-factors equations developed for homogeneous materials.

Figure 9 compares the *J*-resistance curves for the shallow crack SE(B) specimen and SE(T) configuration with $H/W = 10$ based on η-factors for homogeneous materials and overmatched welds as represented by open and solid symbols. The η-values for the overmatch condition are determined from using the estimation Eqs.(8-11) with M_y = 1,18. Again, to facilitate comparison, only the lowest and highest resistance curves for these crack configurations are included in the plot. The trend is clear. The fracture resistance curves derived from η-factors for overmatched welds are practically indistinguishable from the curves evaluated with η-factors for homogeneous materials. Here, use of η-factors for homogeneous materials (*i.e.*, not taking into account the degree of weld strength overmatch) leads to slightly nonconservative (higher) estimates of the resistance curve (we should emphasize that the larger the levels of weld strength mismatch the larger the degree of nonconservativeness).

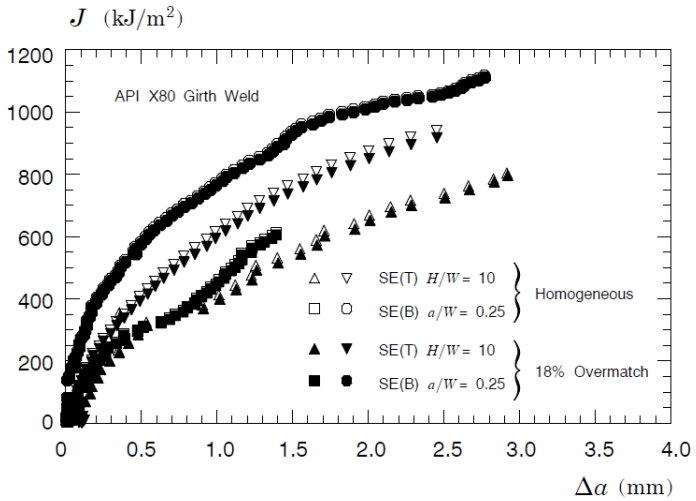

Figure 9 *Effects of 18% weld strength mismatch on J-R curves for the tested X80 pipeline girth weld using clamped, H/W=10 SE(T) and shallow crack SE(B) specimens*

Crack Extension Estimates

To verify the accuracy of fracture resistance measurement, a quantitative examination was performed for each specimen in order to validate the tests according to ASTM E1820 Standard [5]. The criterion pertinent to this discussion about specimen validity according to ASTM E1820 is the optical crack size measurement. As described in Section 8.5.4 of the standard [5], it is necessary that "…none of the nine measurements of original crack size ($a_{0\text{-}i}$) and final physical crack size ($a_{p\text{-}i}$) may differ by more than $0.05B$ from the average physical crack sizes (respectively a_0 and a_p) defined in 8.5.3…". The aforementioned average physical crack sizes are evaluated by this standard using Eq. (25), which is presented here for the original crack size a_0 but can be equally applied to a_p. Here. a_i represents each one of nine equally spaced measurements along the crack front, as illustrated by Figure 10. From the base of the specimen presented by this figure, $a_{0\text{-}i}$ are illustrated using round open markers and $a_{p\text{-}i}$ using triangular open markers.

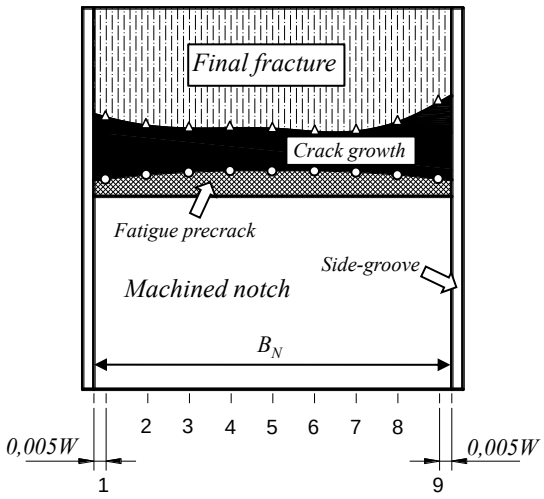

Figure 10 *Measurement scheme of physical crack front according to ASTM E1820 – 9 equally spaced points. The same procedure was conducted using computational image analysis based on several points equally spaced by 0.15 mm.*

$$a_0 = \frac{\left(\frac{a_{0-1} + a_{0-9}}{2}\right) + \sum_{i=2}^{n-1} a_{0-i}}{n-1} \qquad (25)$$

Table 2 provides the predicted and measured crack extension for all tested fracture specimens. The significant features that emerge from these results include: (1) predictions of crack extension based on the UC procedure for the SE(T) specimens are in close agreement with experimental measurements with a level of accuracy of ±5%; (2) crack growth estimates for the C(T) specimen by unloading compliance also display nearly the same accuracy as the SE(T) specimens; (3) crack extension predictions for the shallow crack SE(B) configuration derived from the UC procedure are not in good agreement with the measured amount of ductile tearing; here, the unloading compliance method underestimates the 9-point average crack extension by 25-30% which produces apparent higher *J*-resistance curves.

Table 2 *Final crack length estimation based on UC procedure.*

ID	a_0, mm	a_p, mm		Dev. (%)
		Measured	Predicted	
SE(B) Specimens				
1	4.45	6.35	5.85	**26.32**
2	5.08	7.03	6.55	**24.53**
3	4.34	6.68	6.12	**23.85**
4	3.65	7.56	6.29	**32.65**
5	3.72	7.82	6.53	**31.28**
SE(T) Specimens				
1 $_{H/W\ 10}$	5.66	8.79	8.77	**0.78**
2 $_{H/W\ 10}$	6.11	8.66	8.56	**3.87**
3 $_{H/W\ 10}$	6.29	9.32	9.20	**3.75**
4 $_{H/W\ 10}$	6.70	10.59	10.59	**0.03**
1 $_{H/W\ 6}$	6.90	10.39	10.56	**-4.90**
2 $_{H/W\ 6}$	6.64	10.16	10.19	**-0.73**
3 $_{H/W\ 6}$	6.26	10.13	10.06	**1.74**
C(T) Specimens				
1	28.21	30.85	28.64	**0.13**
2	27.60	34.16	34.54	**-7.36**

This last feature deserves further discussion. The UC procedure described previously to estimate the current crack length involves the assumption of a straight crack front. Consequently, the compliance equations discussed in "Estimation Procedure" Section should be viewed as idealized solutions providing estimates for the average crack extension. To a certain degree, the crack growth behavior for the shallow crack SE(B) configuration can be explained in terms of the uneven crack advance and a rather irregular crack front profile observed in these specimens. To illustrate this issue, Figures 11 and 12 shows the distribution of the measured final crack length, a_f, along the crack front (Z = 0 marks the center of specimen thickness) of two representative fracture specimens for the SE(T) and SE(B) configurations, respectively. In these plots, the solid symbols denote the 9-point experimental measurements and the corresponding average values are defined by dashed and solid lines. With exception of measured points lying near the side-groove (Z = ±6.25 mm), it can be seen that the SE(T) specimen displays a rather more uniform crack extension than the SE(B) specimen (notice that the scales are the same in the plots). Moreover, and perhaps more importantly, the inaccurate estimate of crack extension resulting from these analyses is suggestive of a strong effect of the bend loading mode on crack length predictions.

Indeed, previous studies [33,34] have already indicated that use of the UC method with three-point bend specimens underestimates crack extension when compared with optically measured values of crack length; this effect appears to be more pronounced for SE(B) configurations with reduced size such as the bend specimen geometry used in the present work.

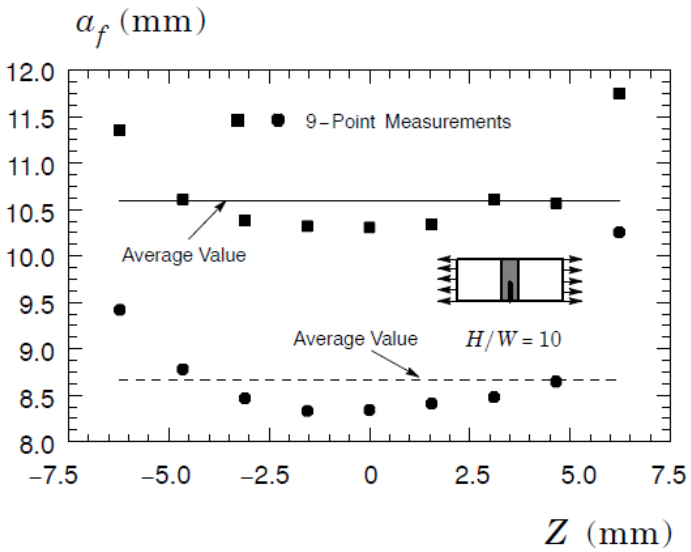

Figure 11 *Evaluation of physical crack front measurements and straightness of crack front validation test for SE(T) specimens according to ASTM E1820*

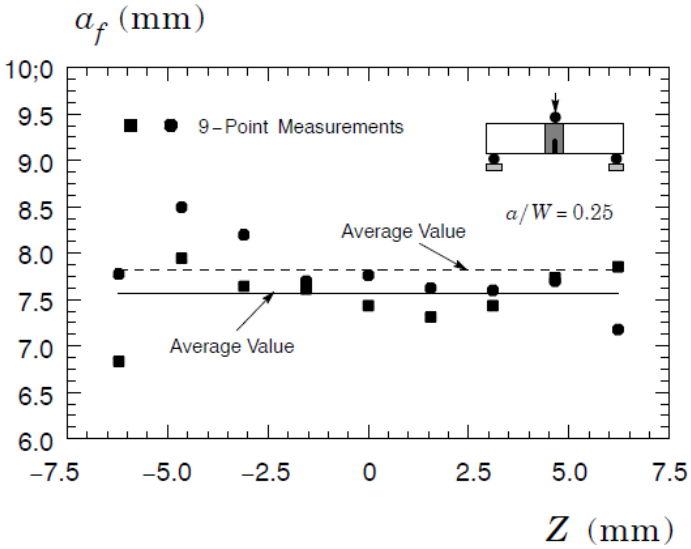

Figure 12 *Evaluation of physical crack front measurements and straightness of crack front validation test for SE(T) specimens according to ASTM E1820*

CONCLUDING REMARKS

This study describes an experimental investigation of the ductile tearing properties for a girth weld made of an API 5L X80 pipeline steel using experimentally measured crack growth resistance curves (*J-Δa* curves). Testing of the pipeline girth welds utilized side-grooved, clamped SE(T) specimens and shallow crack bend SE(B) specimens with a weld centerline notch to determine the crack growth resistance curves based upon the unloading compliance (UC) method using a single specimen technique. The work described here supports the

following conclusions: (1) shallow crack SE(B) specimens provide crack growth resistance curves which are comparable to *J*-resistance curves for clamped SE(T) specimens. Despite the relatively larger scatter of the *J*-Δa data, the fracture resistance for the shallow crack SE(B) configuration at a fixed amount of crack growth, Δa, is similar to the corresponding fracture resistance for the SE(T) specimen; (2) There is little influence of the clamp distance, *H*, on the *J*-*R* curves for the clamped SE(T) specimen configuration within the tested *H/W* range; (3) Levels of weld strength overmatch within the range of 10-20% overmatch do not affect significantly *J*-resistance curves derived from using η-values applicable to homogeneous materials. While the fracture resistance curves based on η-values for homogeneous materials are slightly higher than the corresponding curves based on η-factors for overmatched weldments, differences are nevertheless small and within acceptable limits; (4) Crack extension predictions based on the UC procedure agree well with experimental measurements for the SE(T) and C(T) specimens. In contrast, the unloading compliance method underestimates the 9-point average crack extension for the shallow crack SE(B) specimen by 25-30%. This rather strong underprediction of crack extension for this crack configuration produces apparent higher *J*-resistance curves and, at the same time, underlies some limitations of current UC estimation equations to predict crack length in small size bend specimens.

While the analyses described here clearly provide support to use shallow crack bend specimens as an alternative fracture specimen to measure crack growth properties for pipeline girth welds and similar structural components, they are also suggestive of the need for more experimental studies to validate the UC-based procedure for estimating *J*-resistance curves of SE(B) configurations. In particular, more accurate techniques for crack length estimations in small size bend specimens appear central to develop a robust and effcient *J*-resistance evaluation procedure. Additional work is in progress along these lines of investigation.

ACKNOWLEDGMENTS

This investigation is supported by the Brazilian Science and Technology Ministry (MCT), FINEP and by Agência Nacional de Petróleo e Gás Natural (ANP), through PRH/ANP-MCT 19 agreement. The authors acknowledge Tenaris-Confab, Lincoln Electric Brasil, FEI University and SENAI for providing support for the experiments described in this work.

REFERENCES

[1] S. Manouchehri, B. Howard, S. Denniel, “A discussion of the effect of the reeled installation process on pipeline limit states”, in: 18th International Offshore and Polar Engineering Conference (ISOPE) , Vancouver, Canada, 2008.

[2] S. Wästberg, H. Pisarski, B. Nyhus, “Guidelines for Engineering critical assessments for pipeline installation methods introduzing cyclic plastic strain”, in: 23rd International Conference on Offshore Mechanics and Arctic Engineering (OMAE), Vancouver, Canada, 2004.

[3] J. W. Hutchinson, Fundamentals of the phenomenological theory of nonlinear fracture mechanics, Journal of Applied Mechanics 50 (1983) 1042-1051.

[4] T. L. Anderson, Fracture Mechanics: Fundaments and Applications - 3rd Edition, CRC Press, Boca Raton, FL, 2005.

[5] American Society for Testing and Materials, Standard test method for measurement of fracture toughness, ASTM E1820-2011 (2011).

[6] Det Norske Veritas, Fracture control for pipeline installation methods introducing cyclic plastic strain, DNV-RP-F108 (2006).

[7] S. Cravero, C. Ruggieri, “Estimation procedure of J-resistance curves for SE(T) fracture specimens using unloading compliance”, Engineering Fracture Mechanics 74 (2007) 2735-2757.

[8] S. Cravero, C. Ruggieri, “Further developments in J evaluation procedure for growing cracks based on LLD and CMOD data”, International Journal of Fracture 148 (2007) 347-400.

[9] G. Shen, W. R. Tyson, “Crack size evaluation using unloading compliance in single-specimen single-edge notched tension fracture toughness testing”, Journal of Testing and Evaluation 37 (4) (2009) JTE102368.

[10] B. Nyhus, M. Polanco, O. Ørjasæter, SENT specimens as an alternative to SENB specimens for fracture mechanics testing of pipelines, in: 22nd International Conference on Ocean, Offshore and Arctic Engineering (OMAE) , Vancouver, Canada, 2003.

[11] S. Cravero, C. Ruggieri, “Correlation of fracture behavior in high pressure pipelines with axial flaws using constraint designed test specimens - Part I: Plane-strain analyses”, Engineering Fracture Mechanics 72 (2005) 1344-1360.

[12] L. A. L. Silva, S. Cravero, C. Ruggieri, “Correlation of fracture behavior in high pressure pipelines with axial flaws using constraint designed test specimens - Part II: 3-D effects on constraint”, Engineering Fracture Mechanics 76 (2006) 2123-2138.

[13] G. Shen, R. Bouchard, J. A. Gianetto, W. R. Tyson, “Fracture toughness evaluation of high-strength steel pipe”, in: ASME PVP 2008 Pressure Vessel and Piping Division

Conference, American Society of Mechanical Engineers, Chicago, IL, 2008.

[14] D. Y. Park, W. R. Tyson, J. A. Gianetto, G. Shen, R. S. Eagleson, “Evaluation of fracture toughness of X100 pipe steel using SE(B) and clamped SE(T) single specimens”, in: 8th International Pipeline Conference (IPC) , Calgary, Canada, 2010.

[15] American Society for Testing and Materials, Standard test and definitions for mechanical testing of steel products, ASTM A370-09a, 2009.

[16] American Petroleum Institute, API Standard 579-1/ASME FFS-1, Fitness-For-Service, Second Edition, 2007.

[17] H. Tada, P. C. Paris, G. R. Irwin, The Stress Analysis of Cracks Handbook, 3rd Edition, American Society of Mechanical Engineers, 2000.

[18] H. A. Ernst, P. C. Paris, J. D. Landes, “Estimations on J-integral and tearing modulus T from a single specimen record”, in: R. Roberts (Ed.), Fracture Mechanics: Thirteenth Conference, ASTM STP 743, American Society for Testing and Materials, Philadelphia, 1981, pp. 476-502.

[19] X. K. Zhu, B. N. Leis, J. A. Joyce, “Experimentation estimation of J-R curves from load-CMOD record for SE(B) specimens”, Journal of ASTM International 5 (5) (2008) JAI101532.

[20] J. A. Joyce, E. M. Hackett, C. Roe, “Effects of crack depth and mode loading on the J-R curve behavior of a high strength steel”, in: J. H. Underwood, K.-H. Schwalbe, R. H. Dodds (Eds.), Constraint Effects in Fracture, ASTM STP 1171, American Society for Testing and Materials, Philadelphia, 1993, pp.239-263.

[21] C. Ruggieri, “Further results in J and CTOD estimation procedures for SE(T) fracture specimens – Part I: Homogeneous materials”, Engineering Fracture Mechanics 79 (2012) 245-265.

[22] M. Paredes, C. Ruggieri, “Further results in J and CTOD estimation procedures for SE(T) fracture specimens - Part II: weld centerline cracks”, Engineering Fracture Mechanics 89 (2012) 24-39.

[23] M. T. Kirk, R. H. Dodds, “J and CTOD estimation equations for shallow cracks in single edge notch bend specimens”, Journal of Testing and Evaluation 21 (1993) 228-238.

[24] Y. J. Kim, K.-H. Schwalbe, “On experimental J estimation equations based on CMOD for SE(B) specimens”, Journal of Testing and Evaluation 29 (2001) 67-71.

[25] G. H. B. Donato, C. Ruggieri, “Estimation procedure for J and CTOD fracture parameters using three point bend specimens”, in: 6th International Pipeline Conference (IPC 2006) , Calgary, Canada, 2006.

[26] X. K. Zhu, J. A. Joyce, “Revised incremental J-integral equations for ASTM E1820 using the crack mouth opening displacement”, Journal of Testing and Evaluation 37 (3) (2009) JTE102183.

[27] J. R. Petti, R. H. Dodds, L. R. Link, Crack mouth opening displacement-based Eta factors for SE(B) specimens, Journal of Testing and Evaluation 37 (4) (2009) 14.

[28] J. A. Begley, J. D. Landes, “The J-integral as a fracture criterion”, in: H. T. Corten, J. P. Gallagher (Eds.), Fracture Toughness, ASTM STP 514, American Society for Testing and Materials, Philadelphia, 1972, pp. 120.

[29] American Society for Testing and Materials, Standard test methods for linear-elastic plane-strain fracture toughness K_{Ic} of metallic materials, ASTM E399-2009 (2009).

[30] R. G. Savioli, C. Ruggieri, J and CTOD estimation formulas for C(T) fracture specimens including eects of weld strength overmatch, International Journal of Fracture 179 (2013) 109-127.

[31] C. Ruggieri, “FRACTUS2D: Numerical computation of fracture mechanics parameters for 2-D cracked Solids”, Tech. rep., University of Sao Paulo (2011).

[32] G. H. B. Donato, R. Magnabosco, C. Ruggieri, Eects of weld strength mismatch on J and CTOD estimation procedure for SE(B) specimens, International Journal of Fracture 159 (2009) 120.

[33] P. A. J. M. Steekamp, “J-R curve testing of three-point bend specimen by the unloading compliance method”, in: D. T. Read, R. P. Reed (Eds.), Fracture Mechanics: Eighteenth Symposium, ASTM STP 945, American Society for Testing and Materials, Philadelphia, 1988, pp. 583-610.

[34] J. Dzugan, “Crack length calculation by the unloading compliance technique for charpy size specimens”, Wissenschaftlich-Technische Berichte FZR-385, Forschungszentrum Rossendorf (FZR) (2003).

